

## Three New Late-type Hypervelocity Star Candidates from *Gaia* DR2 with Refined Selection Criteria

Jiao Li<sup>1,2,3,4</sup>, Shi Jia<sup>5,1,2</sup>, Yan Gao<sup>1,2,3,4</sup>, Deng-Kai Jiang<sup>1,2,4</sup>, Thomas Kupfer<sup>6,7</sup>, Ulrich Heber<sup>8</sup>, Chao Liu<sup>9</sup>, Xue-Fei Chen<sup>1,2,4</sup> and Zhan-Wen Han<sup>1,2,3,4</sup>

<sup>1</sup> Yunnan observatories, Chinese Academy of Sciences, Kunming 650011, China; [lijiao@ynao.ac.cn](mailto:lijiao@ynao.ac.cn), [sjia@must.edu.mo](mailto:sjia@must.edu.mo), [zhanwenhan@ynao.ac.cn](mailto:zhanwenhan@ynao.ac.cn)

<sup>2</sup> Key Laboratory for the Structure and Evolution of Celestial Objects, Yunnan observatories, Chinese Academy of Sciences, Kunming 650011, China

<sup>3</sup> University of Chinese Academy of Sciences, Beijing 100049, China

<sup>4</sup> Center for Astronomical Mega-Science, Chinese Academy of Sciences, Beijing 100101, China

<sup>5</sup> State Key Laboratory of Lunar and Planetary Sciences, Macau University of Science and Technology, Macau, China

<sup>6</sup> Kavli Institute for Theoretical Physics, University of California, Santa Barbara, CA 93106, USA

<sup>7</sup> Department of Physics, University of California, Santa Barbara, CA 93106, USA

<sup>8</sup> Dr. Remeis-Sternwarte & ECAP, University of Erlangen-Nürnberg, Erlangen, Germany

<sup>9</sup> Key Lab of Optical Astronomy, National Astronomical Observatories, Chinese Academy of Sciences, Beijing 100101, China

Received 2019 September 29; accepted 2019 November 13

**Abstract** Several dozen hypervelocity star (HVS) candidates have been reported based on the second data release of *Gaia* (*Gaia* DR2). However, it has been proven that the radial velocities of some *Gaia* HVS candidates are not reliable. In this paper, we employ refined astrometric criteria to re-examine *Gaia* DR2, arriving at a more reliable sample of HVS and high velocity star candidates than those found by previous authors. We develop a method called Binary Escape Probability Analysis to identify some HVS candidates. This method allows us to work with stars having only two epochs of measured radial velocity. These stars were usually discarded in previous similar studies. A scrutiny of our final results sheds light on selection effects present in our studies, which we propose to be the focus of future studies. In total, we find three late-type (2 G-type and 1 K-type) HVS and 21 high velocity star candidates, 3 and 11 of which are new, respectively. Judging by their historical trajectories, which we calculate, all three HVS candidates could not have had Galactic center origins. Further monitoring is required to confirm their status.

**Key words:** stars: kinematics and dynamics — evolution — statistics

### 1 INTRODUCTION

Hyper-velocity stars (HVSs)<sup>1</sup> are important tools for probing the Galactic structure (e.g., Kenyon et al. 2008; Lu et al. 2010; Kenyon et al. 2014; Brown 2015). HVSs, which were first theoretically predicted by Hills (1988), are usually defined as stars which can escape the gravitational potential of the Milky Way (MW). Since the first HVS was discovered in 2005 (Brown et al. 2005), some further HVS candidates have been found in recent years

(e.g., Edelmann et al. 2005; Hirsch et al. 2005; Brown 2006; Brown et al. 2009, 2012, 2014; Tillich et al. 2009; Li et al. 2012; Palladino et al. 2014; Zheng et al. 2014; Zhong et al. 2014; Geier et al. 2015; Li et al. 2015; Huang et al. 2017). However, several of the late type HVS candidates have been rejected from ground based astrometry (Ziegerer et al. 2015). These candidates cover a wide range of spectral types from OBA stars to FGK stars (see the open fast stars catalog from Boubert et al. 2018). However, the origin of HVSs is still unclear. According to current understanding (see the review Brown 2015), HVSs may have either been formed in the Galaxy or an extragalactic source.

---

<sup>1</sup> HVSs are generally thought to be the stars ejected by the Galaxy's central massive black hole at speeds that can potentially unbind them from the Galaxy. In our paper, we define all unbound stars as HVSs, for the sake of simplicity.

The high velocity of HVSs can be attributed to a number of different ejection mechanisms. The mainstream mechanism is the dynamical interactions between stars and the supermassive central black hole of the MW (e.g., Hills 1988; Yu & Tremaine 2003; Zhang et al. 2010), which corresponds to an origin at the Galactic center (GC). The kinematic properties of S5-HVS1 is consistent with a GC origin (Koposov et al. 2019). Alternatively, a fraction of HVSs originate from the Galactic disk (Irrgang et al. 2018). These can be produced via supernova explosions in close binary systems (e.g., Blaauw 1961; Tauris & Takens 1998; Wang & Han 2009; Tauris 2015) or via dynamical ejections in multiple stellar systems (e.g., Gvaramadze et al. 2009). For example, HVS2 (also known as US 708) is likely to be the surviving companion star of a helium double-detonation Type Ia supernova (Wang et al. 2013; Geier et al. 2015). In addition, the hypervelocity white dwarf (HVWD) LP 40-365 (Vennes et al. 2017; Raddi et al. 2018a,b) and three newly discovered HVWD candidates (Shen et al. 2018) may also be related to the surviving companions of Type Ia supernovae. Besides ejection from the MW, HVSs could also originate from disrupted dwarf galaxies (e.g., Abadi et al. 2009) or the Large Magellanic Cloud (LMC) (e.g., Boubert & Evans 2016; Boubert et al. 2017). Recently, the B star HE 0437-5439 (HVS3) was found to have a high probability of originating in the LMC (Irrgang et al. 2018; Erkal et al. 2019) as already proposed by Edelmann et al. (2005).

So far, the population of confirmed HVSs is dominated by OBA-type stars (Brown 2015; Erkal et al. 2019; Boubert et al. 2018). Estimating the total velocities of these confirmed HVSs relative to the GC has thus far been achieved via their radial velocities alone, due to the difficulties of measuring proper motion precisely. However, a star’s tangential velocity (proper motion times distance) can also contribute significantly to its total velocity (Palladino et al. 2014; Ziegerer et al. 2015). The European Space Agency satellite *Gaia* has made it possible to search for new HVS candidates and to investigate the origins of HVSs with higher-precision proper motion and stellar property measurements (Evans et al. 2018; Gaia Collaboration et al. 2018a; Marchetti et al. 2018a).

Armed with this new instrument and the knowledge of an observed object’s tangential velocity that accompanied it, it was not long before our understanding of HVSs was enhanced. Brown et al. (2018), Erkal et al. (2019), and Irrgang et al. (2018) all studied the origins of known HVSs by obtaining the three-dimensional velocities of these objects from their radial and tangential velocities, and extrapolating back in time to see where they came from. Historical archives of possible HVS candidates, generated from a mixture of spectroscopic radial velocities and

very crude tangential velocity estimates, were also revisited (Boubert et al. 2018). Many of the objects among them, including the hot subdwarfs US 708 (Hirsch et al. 2005; Geier et al. 2015) and SDSS J013655.91+242546.0 (Tillich et al. 2009) as well as LP40-365 (GD 492, Vennes et al. 2017; Raddi et al. 2018b) and the LAMOST F9 dwarf star Li10 (Li et al. 2015), were confirmed to be HVSs. Then Raddi et al. (2019) find other two WD HVS which is similar to LP40-365. Other studies concentrated on systematic searches for new HVS candidates among the *Gaia* DR2 data (e.g. Bromley et al. 2018; Marchetti et al. 2019; Du et al. 2019), and indeed many were found. However, it should be noted here that these new HVS candidates were identified using *Gaia* DR2 radial and tangential velocities, the former of which was found to be spurious in some cases due to contamination from neighboring objects (Boubert et al. 2019), and the latter of which did not undergo an efficient test of reliability (see below for details). This led to uncertainties among the candidate selection criteria. Further compounding the issue is the fact that different Galactic potential models can also lead to marginally different results as to whether a certain object can escape, given its current position and velocity. The uncertainty introduced by different Galactic potential models can be at least partly remedied by meticulously listing all the high velocity stars, which have not quite achieved hypervelocity status, found by each study, and by cross-referencing these lists with those of other studies. Establishing these lists may have other benefits, as stars travelling at abnormally high velocities are interesting in their own right, even when they have not achieved escape velocity (Capuzzo-Dolcetta & Fragione 2015). However, even this measure does not obviate the need of refining the selection criteria of HVS candidates, leading to efficient identification of less controversial HVS candidates with as little data wasted as possible, hence this paper.

To improve the identification efficiency of the selection criteria, three measures can be taken. During the initial candidate selection phase, it is wise to ascertain that the proper motion and parallax model fits to *Gaia* data are reliable for the sample. We accomplish this by taking advantage of recent studies that have shown that the *RUWE* (re-normalised unit weight error) statistic (Lindgren et al. 2018) is a good indicator of this reliability. The issue of potential binarity among the sample stars can also be more elegantly handled, such that objects which would have enough velocity to escape the Galaxy, even if contamination due to binarity were to be considered, need not be eliminated from the sample. We achieve this by means of BEPA (Binary Escape Probability Analysis), which is an analytical method that we have developed. The details of BEPA will be given later on. Finally, the aforementioned contami-

nation in the spectra used for radial velocity determination can also be addressed, by simply eliminating those stars which suffer from this influence. In this paper, we adopt all three.

In this work, we first select the HVS candidates and high velocity star candidates from *Gaia* DR2 catalogues (Sect. 2). Initially, we obtain 16 HVS candidates and 23 high velocity star candidates. In Section 3, we develop the BEPA approach to study the unbound probabilities of our HVS candidates if they were binary systems, especially for the candidates with only two measured radial velocity epochs from *Gaia* ( $rv\_nb\_transits = 2$ ). In Section 4, we analyze the reliability of the radial velocities of our candidates. Then, we discuss the implications of our work for future studies and the origins of our HVS candidates in Section 5. Finally, we conclude with a summary.

## 2 METHOD

### 2.1 The Galactic Space Velocities

*Gaia* DR2 contains 1 692 918 784 sources, of which 7 224 631 have median radial velocities and effective temperatures in the range of [3550, 6900] K (Katz et al. 2019). We select the sources with parallaxes larger than 5 times parallax errors ( $\varpi > 5\sigma_\varpi$ ), the distances of which we directly determine by inverting their parallaxes:  $d = 1/\varpi$  (Astraatmadja & Bailer-Jones 2016). We assume that the Sun is located on the Galactic disk at  $z = 0$ , at a distance of  $d_\odot = 8.27$  kpc from the GC, that its peculiar velocity relative to the GC is  $(U_\odot, V_\odot, W_\odot) = (11.1, 12.24, 7.25)$  km s<sup>-1</sup>, and that the local circular speed of the Sun is  $V_c = 238$  km s<sup>-1</sup> (Schönrich et al. 2010; Schönrich 2012). Then, we use the *Gaia* astrometric parameters and their associated errors, which we process using TOPCAT (<http://www.star.bris.ac.uk/~mbt/topcat/>) (Taylor 2005), to calculate the Galactic rest frame positions and velocities  $v_{grf}$  for the sources with radial velocities.

### 2.2 Selection Criteria

To filter out data processing artifacts and spurious measurements, we use the following selection criteria:

- (a)  $\varpi > 5\sigma_\varpi$
- (b)  $-0.23 \leq \text{mean\_varpi\_factor\_al} \leq 0.32$
- (c)  $\text{visibility\_periods\_used} > 8$
- (d)  $\text{astrometric\_excess\_noise\_sig} \leq 2$
- (e)  $\text{astrometric\_gof\_al} < 3$
- (f)  $\text{phot\_g\_mean\_flux\_over\_error} > 20$
- (g)  $\text{phot\_bp\_mean\_flux\_over\_error} > 20$

(h)  $\text{phot\_rp\_mean\_flux\_over\_error} > 20$

(i)  $\frac{\text{phot\_bp\_rp\_excess\_factor}}{1.2 + 0.03(\text{phot\_bp\_mean\_mag} - \text{phot\_rp\_mean\_mag})^2} < 1.2$

(j)  $v_{grf} > v_{esc}$  or  $v_{min} > v_{esc}$

(k)  $RUWE < 1.4$

Criteria (a), (b) and (c) ensure that the parallaxes are precise and not vulnerable to errors (Astraatmadja & Bailer-Jones 2016). Criteria (d) and (e) eliminate sources which yield bad astrometric fits (Gaia Collaboration 2018; Gaia Collaboration et al. 2018a, details can be found in the *Gaia* Columns description [https://gea.esac.esa.int/archive/documentation/GDR2/Gaia\\_archive/chap\\_datamodel/sec\\_dm\\_main\\_tables/ssc\\_dm\\_gaia\\_source.html](https://gea.esac.esa.int/archive/documentation/GDR2/Gaia_archive/chap_datamodel/sec_dm_main_tables/ssc_dm_gaia_source.html)). Criteria (f), (g), (h) and (i) select sources with good photometry (Evans et al. 2018; Gaia Collaboration et al. 2019), which do not suffer from contamination from nearby sources, and provide relatively good astrometric measurements and radial velocities. Criterion (k) makes sure that the *Gaia* astrometric five-parameter solution is “good”. *RUWE* is the re-normalised unit weight error described by Lindegren et al. (2018) and calculated with the corresponding lookup tables provided at <https://www.cosmos.esa.int/web/gaia/dr2-known-issues>. It is the equivalent of a reduced  $\chi^2$  statistic for the five-parameter solution fit. It should be noted that this last criterion was not applied in any previous study in this field to date.

Currently, there are several competing Galactic potential models. For different models, the escape speed can differ by hundreds of kilometers per second, as shown in Figure 1. For our preliminary candidate selection, which should ideally include as many objects as possible, we use the lightest gravitational potential model of Allen & Santillan (1991) to calculate their escape velocities  $v_{esc}$ , and follow up with Potential Model I of Irrgang et al. (2013) later in our paper for more stringent constraints. After applying criteria (a)-(k), we arrive at 84 candidates. We then use a Monte Carlo (MC) method to estimate their probabilities of being unbound.

### 2.3 Probabilities of Being Unbound

We model the coordinate, parallax and proper motion distributions as a multivariate Gaussian distribution with a mean vector  $\mathbf{m}$  and covariance matrix  $\Sigma$  (see Eq. (1), as well as Eq. (2)):

$$\mathbf{m} = (\alpha, \delta, \varpi, \mu_\alpha, \mu_\delta), \quad (1)$$

where  $\alpha, \delta, \varpi, \mu_\alpha, \mu_\delta$  are the right ascension, declination, parallax, and proper motions in the direction of the right ascension and declination, respectively;

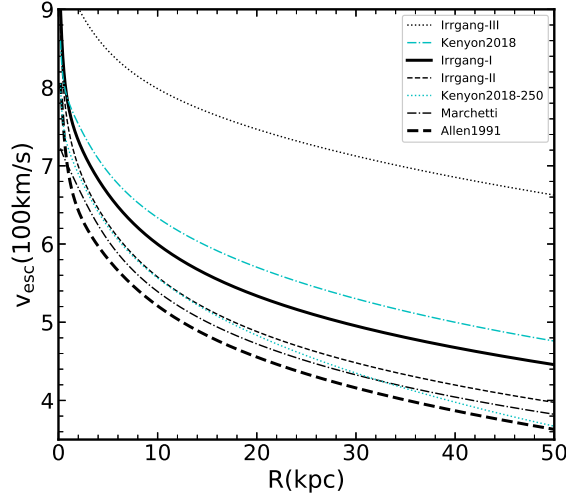


**Fig. 1** The escape speed curves based on different Galactic potential models at the Galactic disk plane ( $z = 0$ ). Irrgang-I, II, and III are obtained from the potential models of Allen & Santillan (1991), Wilkinson & Evans (1999) and Navarro et al. (1997), respectively, and the parameters of these models are updated by Irrgang et al. (2013); both of Kenyon2018 and Kenyon2018-250 are based on the potential model of Kenyon et al. (2018), but their escape speeds are calculated by  $\sqrt{-2\varphi(\mathbf{r}_{GC})}$  and  $\sqrt{2[\varphi(250 \text{ kpc}) - \varphi(\mathbf{r}_{GC})]}$ , respectively; Marchetti is from the potential model used in Marchetti et al. (2019); Allen1991 is calculated with the potential model and parameters of Allen & Santillan (1991). It should be noted here that the huge escape velocity of Irrgang-III is at odds with observational results (Irrgang et al. 2018).

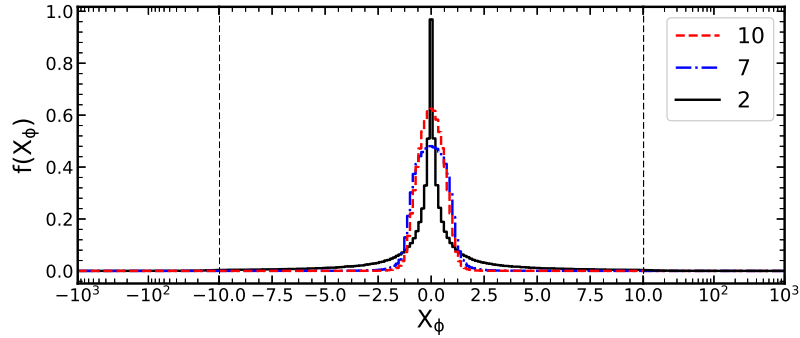


**Fig. 2** The probability density of  $X_\phi$  for MC simulations with simulated number of observations of 2, 7, and 10, respectively. This provides an estimate of the actual values of  $X_\phi$  encountered in the *Gaia* observations. Note that the horizontal axis is linear within the vertical dashed lines, and logarithmic beyond them.

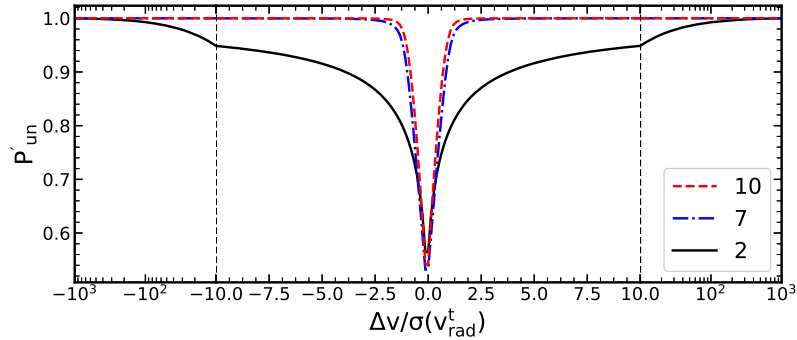


**Fig. 3** The escape probabilities or a series of values of  $\frac{\Delta v}{\sigma(v_{\text{rad}}^t)}$ , where  $\Delta v = v_{\text{rad}} - v_{\text{resc},i}$ , ( $i = 1, 2$ ),  $v_{\text{rad}}$  and  $\sigma(v_{\text{rad}}^t)$  are the median and standard deviation of the radial velocities of *Gaia* DR2, respectively. Note that the horizontal axis is linear within the vertical dashed lines, and logarithmic beyond them.

$$\Sigma = \begin{pmatrix} \sigma_\alpha \sigma_\alpha & \sigma_\alpha \sigma_\delta \rho(\alpha, \delta) & \sigma_\alpha \sigma_\varpi \rho(\alpha, \varpi) & \sigma_\alpha \sigma_{\mu_\alpha} \rho(\alpha, \mu_\alpha) & \sigma_\alpha \sigma_{\mu_\delta} \rho(\alpha, \mu_\delta) \\ \sigma_\delta \sigma_\alpha \rho(\delta, \alpha) & \sigma_\delta \sigma_\delta & \sigma_\delta \sigma_\varpi \rho(\delta, \varpi) & \sigma_{\delta \mu_\alpha} \rho(\delta, \mu_\alpha) & \sigma_\delta \sigma_{\mu_\delta} \rho(\delta, \mu_\delta) \\ \sigma_\varpi \sigma_\alpha \rho(\varpi, \alpha) & \sigma_\varpi \sigma_\delta \rho(\varpi, \delta) & \sigma_\varpi \sigma_\varpi & \sigma_\varpi \sigma_{\mu_\alpha} \rho(\varpi, \mu_\alpha) & \sigma_\varpi \sigma_{\mu_\delta} \rho(\varpi, \mu_\delta) \\ \sigma_{\mu_\alpha} \sigma_\alpha \rho(\mu_\alpha, \alpha) & \sigma_{\mu_\alpha} \sigma_\delta \rho(\mu_\alpha, \delta) & \sigma_{\mu_\alpha} \sigma_\varpi \rho(\mu_\alpha, \varpi) & \sigma_{\mu_\alpha} \sigma_{\mu_\alpha} & \sigma_{\mu_\alpha} \sigma_{\mu_\delta} \rho(\mu_\alpha, \mu_\delta) \\ \sigma_{\mu_\delta} \sigma_\alpha \rho(\mu_\delta, \alpha) & \sigma_{\mu_\delta} \sigma_\delta \rho(\mu_\delta, \delta) & \sigma_{\mu_\delta} \sigma_\varpi \rho(\mu_\delta, \varpi) & \sigma_{\mu_\delta} \sigma_{\mu_\alpha} \rho(\mu_\delta, \mu_\alpha) & \sigma_{\mu_\delta} \sigma_{\mu_\delta} \end{pmatrix}, \quad (2)$$

where  $\sigma_i$  is the error of the astrometric parameter  $i$  ( $i = \alpha, \delta, \varpi, \mu_\alpha, \mu_\delta$ ), and  $\rho(i, j) = \rho(j, i)$  denotes the correlation coefficients between the astrometric parameters  $i$  and  $j$ , which can be found in the *Gaia* DR2 catalog (for example,  $\rho(\alpha, \delta)$  is labeled as ra\_dec\_corr).

We then obtain the Galactic rest frame velocities and estimate the unbound probabilities by combining radial velocities and radial velocity errors.

Radial velocity is measured independently, and hence we assume that it follows a normal distribution, the mean and standard deviation of which are the median radial velocity  $v_{\text{rad}}$  and the radial velocity uncertainty  $\epsilon_{v_{\text{rad}}}$  of *Gaia* DR2, respectively.

Devising a MC method, we generate a random position and Galactic rest frame velocity  $v_{\text{grf}}$  according to the aforementioned probability distributions for each sample HVS candidate. From the random position, we calculate its corresponding escape velocity  $v_{\text{esc}}$ , and test whether the HVS candidate is unbound for this particular simulation by comparing  $v_{\text{grf}}$  and  $v_{\text{esc}}$ . This process is repeated  $10^6$  times, leading to a probability that this HVS candidate is unbound,

$$P_{\text{un}} = \frac{n(v_{\text{grf}} > v_{\text{esc}})}{10^6}, \quad (3)$$

where  $n$  is the number of simulations in which  $v_{\text{grf}} > v_{\text{esc}}$ .

For the sake of selecting only the sources with reasonable Galactic space velocities, we follow the criterion used by Marchetti et al. (2019):

$$\sigma_{v_{\text{GC}}} / \tilde{v}_{\text{GC}} < 0.2, \quad (4)$$

where  $\tilde{v}_{\text{GC}}$  is the median of  $v_{\text{grf}}$  (or  $v_{\text{min}}$ ) sampled by our previously mentioned MC method, and  $\sigma_{v_{\text{GC}}}$  is the square root of the sum of the lower and upper uncertainties on  $v_{\text{grf}}$  (see Eq. (5)):

$$\sigma_{v_{\text{GC}}} = \sqrt{[Per(v_{\text{GC}}, 16) - \tilde{v}_{\text{GC}}]^2 + [Per(v_{\text{GC}}, 84) - \tilde{v}_{\text{GC}}]^2}, \quad (5)$$

where  $Per(v_{\text{GC}}, 16)$  and  $Per(v_{\text{GC}}, 84)$  are the 16th and the 84th percentiles of  $v_{\text{GC}}$  (or  $v_{\text{min}}$ ), respectively.

After applying this criterion, our sample consists of 39 candidates (see Table 1 and Table 3). To obtain our final HVS candidate sample, we repeat the above procedure for the 39 entries, this time using the Galactic Potential Model I of Irigang et al. (2013), since this model is the most realistic according to recent studies of the motions of globular clusters and satellite galaxies using *Gaia* DR2 astrometry (Gaia Collaboration et al. 2018b; Watkins et al. 2018; Sohn et al. 2018; Fritz et al. 2018). We then proceed

to demand that  $P_{\text{un}} > 0.8$  for all candidates. This yields 16 HVS candidates (defined as *Gaia*-HVSC) with radial velocities (see Tables 1 and 2), and the other 23 sources are defined as high velocity star candidates (defined as HV, see Tables 3 and 4). It should be noticed that, in our analysis above, 15 of the 16 HVS candidates have had their median radial velocities calculated using only two transits ( $rv_{\text{nb\_transits}} = 2$ ). Their apparent radial velocities might be at least partly due to contributions from binary orbits. In the next section, we devise a Binary Escape Probability Analysis (BEPA) approach to derive the probabilities of these HVS candidates being unbound.

### 3 BINARY ESCAPE PROBABILITY ANALYSIS

For sources with only a few observing plane transits, we cannot be certain whether they are components of binary systems. If they were, then binary orbital velocity can manifest itself in the radial velocity measurements, leading to contamination when we are using these radial velocities to calculate whether or not these objects can become unbound from the Galactic potential. To take this possibility into consideration for our unbound probability calculations, we develop the BEPA method, as detailed below.

Assuming that a source is a binary star with an orbital eccentricity of zero, then its radial velocity is composed of systemic and orbital velocities. Its observed median radial velocity can be expressed as

$$\tilde{v}_{\text{rad}} = v_s + \tilde{v}_b^t, \quad (6)$$

where  $v_s$  is the systemic radial velocity, and  $\tilde{v}_b^t$  is the projected velocity in the radial direction due to binary orbital rotation. The radial velocity of the binary is assumed to have a semi-amplitude of  $K$ ,

$$v_b^t = K \cos(\phi^t), \quad (7)$$

where  $\phi^t$  is the orbital phase at the observation epoch  $t$ . We assume that the radial velocity error is due entirely to orbital motion, in which case the standard deviation of the

**Table 1** HVS Candidates with Median Radial Velocities: Basic Source Parameters

<i>Gaia</i> -HVSC	source id	( $\alpha$ , $\delta$ ) J2015.5	$\varpi$ mas	$\mu_\alpha$ mas yr <sup>-1</sup>	$\mu_\delta$ mas yr <sup>-1</sup>	$v_{\text{rad}}$ km s <sup>-1</sup>	( $G$ , $G_{\text{BP}}$ , $G_{\text{RP}}$ ) mag	$T_{\text{eff}}$ K	Type	$N_{B_{\text{rv}}}$
1	5716044263405220096	(115.836451, -19.008715)	$0.52 \pm 0.04$	$-1.26 \pm 0.05$	$-0.76 \pm 0.05$	$-453.5 \pm 2.4$	(15.55, 15.91, 15.02)	$5629^{+629}_{-224}$	G	2
2	5850309098637075328	(206.709336, -68.233936)	$0.32 \pm 0.04$	$-6.68 \pm 0.05$	$-3.57 \pm 0.05$	$-486.9 \pm 5.0$	(15.57, 15.98, 14.98)	$5167^{+187}_{-191}$	G	2
3	5966712023814100736	(255.893150, -41.563702)	$0.79 \pm 0.07$	$1.41 \pm 0.13$	$-3.24 \pm 0.10$	$-967.7 \pm 5.8$	(16.21, 17.08, 15.29)	$4166^{+351}_{-228}$	K	2
4	1825842828672942208	(296.284240, 20.715550)	$0.75 \pm 0.03$	$-0.66 \pm 0.04$	$-5.39 \pm 0.04$	<b><math>641.8 \pm 2.0</math></b>	(14.82, 15.45, 14.03)	$4431^{+113}_{-57}$	K	2
5	2251311188142608000	(301.144379, 70.007552)	$2.89 \pm 0.03$	$4.60 \pm 0.06$	$-3.34 \pm 0.07$	<b><math>738.2 \pm 3.7</math></b>	(15.85, 16.72, 14.87)	$4072^{+126}_{-198}$	K	2
6	4065480978657619968	(273.394905, -24.108792)	$2.34 \pm 0.07$	$-6.33 \pm 0.10$	$-25.18 \pm 0.08$	<b><math>-680.7 \pm 1.9</math></b>	(15.47, 16.24, 14.58)	$4159^{+144}_{-129}$	K	2
7	4076739732812337536	(279.020366, -24.132680)	$0.37 \pm 0.03$	$10.14 \pm 0.05$	$-5.54 \pm 0.05$	<b><math>572.3 \pm 4.8</math></b>	(13.57, 14.25, 12.76)	$4502^{+282}_{-124}$	K	2
8	4103096400926398592	(278.072328, -15.972720)	$0.64 \pm 0.03$	$7.71 \pm 0.06$	$1.25 \pm 0.05$	<b><math>-757.0 \pm 0.7</math></b>	(13.10, 13.79, 12.31)	$4358^{+133}_{-71}$	K	2
9	425659833026724544	(279.866437, -4.972103)	$0.29 \pm 0.03$	$1.16 \pm 0.06$	$-2.03 \pm 0.06$	<b><math>547.6 \pm 1.2</math></b>	(14.34, 15.41, 13.29)	$4007^{+981}_{-422}$	K	2
10	4296894160078561280	(298.560144, 6.421614)	$1.18 \pm 0.05$	$7.44 \pm 0.07$	$-2.10 \pm 0.05$	<b><math>760.0 \pm 1.9</math></b>	(15.65, 16.16, 14.94)	$4870^{+88}_{-45}$	K	2
11	5305975869928712320	(146.227409, -57.568968)	$0.29 \pm 0.02$	$-8.23 \pm 0.04$	$4.79 \pm 0.05$	<b><math>-830.6 \pm 5.6</math></b>	(14.14, 14.76, 13.19)	$4419^{+286}_{-138}$	K	2
12	5412495010218365568	(145.116991, -45.365443)	$1.15 \pm 0.02$	$-6.65 \pm 0.04$	$2.68 \pm 0.04$	<b><math>-474.0 \pm 14.8</math></b>	(14.88, 15.30, 14.29)	$5338^{+112}_{-163}$	G	2
13	5878409248569967972	(217.772803, -61.167859)	$3.06 \pm 0.03$	$32.36 \pm 0.04$	$-0.09 \pm 0.06$	<b><math>-711.9 \pm 3.7</math></b>	(12.30, 12.71, 11.73)	$5342^{+32}_{-35}$	G	2
14	5931224697615320064	(249.224053, -51.719940)	$0.45 \pm 0.03$	$0.50 \pm 0.05$	$-0.74 \pm 0.03$	<b><math>-577.7 \pm 3.7</math></b>	(13.47, 13.69, 13.03)	$6600^{+310}_{-322}$	F	2
15 <sup>B,M</sup>	5932173855446728064	(244.118100, -54.440452)	$0.45 \pm 0.03$	$-2.68 \pm 0.04$	$-4.99 \pm 0.03$	<b><math>-614.3 \pm 2.5</math></b>	(13.81, 14.21, 13.22)	$5322^{+160}_{-124}$	G	7
16	5951114420631264640	(260.139995, -46.794507)	$0.99 \pm 0.05$	$2.68 \pm 0.08$	$2.94 \pm 0.06$	<b><math>-984.3 \pm 3.4</math></b>	(15.50, 15.99, 14.84)	$4938^{+224}_{-109}$	K	2

In the first column, the superscript “B” and “M” indicates the sources which are listed in Bromley et al. (2018) and Marchetti et al. (2019), respectively.  $N_{B_{\text{rv}}}$  is the number of transits used to compute the medians and standard deviations of the radial velocities (rv\_nb\_transits).  $T_{\text{eff}}$  is the effective temperature from the *Gaia* DR2 catalogue. “TYPE” is the spectral type which is roughly estimated from the corresponding *Gaia* DR2 effective temperature. The numbers shown in red are the *Gaia* measurements which are known to be erroneous for reasons given in Sect. 4, shown “as is”, without being corrected to their true physical values. Their unbound probabilities are shown in Table 2.

**Table 2** Unbound Probabilities of HVS Candidates with Median Radial Velocities

<i>Gaia</i> -HVSC	BEPA			1/ $\varpi$				$N_{\text{RP}}$	$N_{\text{G}}$	GOOD	$RUWE$ km s <sup>-1</sup>	$v_{30,\text{esc}}$	$P_{30,\text{un}}$	$P_{\varpi+0.067,\text{un}}$
	$v_{\text{resc}1}$ km s <sup>-1</sup>	$v_{\text{resc}2}$ km s <sup>-1</sup>	$P'_{\text{un}}$	$r_{\text{GC}}$ kpc	$v_{\text{grf}}$ km s <sup>-1</sup>	$v_{\text{esc}}$ km s <sup>-1</sup>	$P_{\text{un}}$							
1	802.59	-377.88	0.978	$9.485^{+0.116}_{-0.098}$	$679^{+2}_{-2}$	$605^{+1}_{-1}$	1.000	0	0	✓	0.947	$605^{+30}_{-30}$	0.993	1.000
2	822.13	-441.45	0.940	$6.819^{+0.094}_{-0.099}$	$680^{+5}_{-5}$	$635^{+1}_{-1}$	1.000	0	0	✓	1.056	$636^{+30}_{-30}$	0.931	1.000
3	642.81	-532.64	0.989	$7.064^{+0.095}_{-0.112}$	$1049^{+6}_{-6}$	$633^{+1}_{-1}$	1.000	0	0	✓	1.051	$633^{+30}_{-30}$	1.000	1.000
4	402.02	-834.64	0.993	$7.632^{+0.022}_{-0.024}$	$863^{+2}_{-2}$	$625^{+0}_{-0}$	1.000	1	1		0.936	$625^{+30}_{-30}$	1.000	1.000
5	376.52	-839.47	0.991	$8.349^{+0.001}_{-0.001}$	$974^{+4}_{-4}$	$617^{+0}_{-0}$	1.000	1	1		1.033	$617^{+30}_{-30}$	1.000	1.000
6	549.01	-633.35	0.972	$7.847^{+0.013}_{-0.014}$	$668^{+2}_{-2}$	$623^{+0}_{-0}$	1.000	1	1		1.000	$623^{+30}_{-30}$	0.932	1.000
7	541.64	-643.60	0.924	$5.660^{+0.185}_{-0.214}$	$681^{+5}_{-5}$	$652^{+3}_{-3}$	1.000	1	0		0.929	$652^{+30}_{-30}$	0.831	1.000
8	493.61	-656.08	0.994	$6.779^{+0.062}_{-0.068}$	$729^{+1}_{-1}$	$636^{+1}_{-1}$	1.000	1	0		0.847	$636^{+30}_{-30}$	0.999	1.000
9	501.30	-749.53	0.981	$5.469^{+0.257}_{-0.309}$	$700^{+1}_{-1}$	$656^{+5}_{-5}$	1.000	1	1		0.881	$656^{+30}_{-30}$	0.925	1.000
10	417.29	-781.86	0.995	$7.715^{+0.020}_{-0.022}$	$959^{+2}_{-2}$	$624^{+0}_{-0}$	1.000	2	2		1.174	$624^{+30}_{-30}$	1.000	1.000
11	851.75	-362.16	0.990	$8.406^{+0.088}_{-0.064}$	$1081^{+6}_{-6}$	$616^{+1}_{-1}$	1.000	0	0		1.202	$616^{+30}_{-30}$	1.000	1.000
12	864.58	-369.26	0.928	$8.294^{+0.002}_{-0.001}$	$722^{+15}_{-15}$	$618^{+0}_{-0}$	1.000	0	0		0.948	$618^{+30}_{-30}$	0.999	1.000
13	746.39	-405.76	0.990	$8.043^{+0.002}_{-0.002}$	$912^{+4}_{-4}$	$620^{+0}_{-0}$	1.000	1	1		1.012	$620^{+30}_{-30}$	1.000	1.000
14	701.16	-501.06	0.969	$6.331^{+0.111}_{-0.125}$	$715^{+3}_{-3}$	$643^{+2}_{-2}$	1.000	1	1		1.153	$643^{+30}_{-30}$	0.991	1.000
15	735.08	-502.80	1.000	$6.461^{+0.101}_{-0.113}$	$749^{+3}_{-3}$	$641^{+2}_{-2}$	1.000	0	1		1.000	$641^{+30}_{-30}$	1.000	1.000
16	639.01	-506.58	0.994	$7.317^{+0.047}_{-0.052}$	$1082^{+3}_{-3}$	$629^{+1}_{-1}$	1.000	0	1		1.044	$629^{+30}_{-30}$	1.000	1.000

$v_{\text{resc}1}$  and  $v_{\text{resc}2}$  are escape velocities in the radial direction (see Sect. 3);  $P'_{\text{un}}$  is the binary escape probability derived by BEPA, i.e., assuming that the source is a binary system;  $r_{\text{GC}}$  is the distance to the Galactic center;  $v_{\text{grf}}$  is the Galactic rest frame velocity;  $v_{\text{esc}}$  is the escape velocity of the Galactic Potential Model I of Irrgang et al. (2013);  $P_{\text{un}}$  is the unbound probability, if its median radial velocity were the systemic radial velocity;  $N_{\text{RP}}$  is the number of stars brighter than the object in question in the  $G_{\text{RP}}$ -band within 6.4 arcsec;  $N_{\text{G}}$  is the number of stars brighter than the object in question in the  $G$ -band within 6.4 arcsec; “GOOD” stands for the candidates with possibly trustworthy radial velocities (detail see Section 4);  $RUWE$  is the re-normalised unit weight error, for which when  $RUWE < 1.4$ , it indicates a “good” solution for astrometric five-parameter fit (Lindgren et al. 2018, <https://www.cosmos.esa.int/web/gaia/dr2-known-issues>). The numbers shown in red are the *Gaia* measurements which are known to be erroneous for reasons given in Sect. 4, shown “as is”, without being corrected to their true physical values;  $P_{30,\text{un}}$  is the unbound probability calculated with  $v_{30,\text{esc}}$ , which is  $v_{\text{esc}}$  with a Gaussian random error of 30 km s<sup>-1</sup> added to it;  $P_{\varpi+0.067,\text{un}}$  is the unbound probability calculated with distance derived by  $1/(\varpi + 0.067 \text{ mas})$ , which considers a *Gaia* parallax offset of  $\sim -0.067 \text{ mas}$  (Arenou et al. 2018).

radial velocity can be expressed as follows,

$$\sigma(v_{\text{rad}}^t) = \sqrt{\frac{1}{N-1} \sum_{t=1}^N (v_{\text{rad}}^t - \frac{1}{N} \sum_{t=1}^N v_{\text{rad}}^t)^2} = K \sigma_{\cos(\phi)}, \quad (8)$$

where  $N$  is the number of observations equal to rv\_nb\_transits. Equation (8) can also be expressed as fol-

lows:

$$\sigma_{\cos(\phi)} = \sqrt{\frac{1}{N-1} \sum_{t=1}^N [\cos(\phi^t) - \frac{1}{N} \sum_{t=1}^N \cos(\phi^t)]^2}. \quad (9)$$

By combining Equations (6), (7) and (9), we find that

$$v_s = \tilde{v}_{\text{rad}} - \sigma(v_{\text{rad}}^t) X_\phi, \quad (10)$$

**Table 3** High Velocity Star Candidates with Median Radial Velocities: Basic Source Parameters

<i>Gaia</i> HVSC	source id	( $\alpha$ , $\delta$ ) J2015.5	$\varpi$ mas	$\mu_\alpha$ mas yr <sup>-1</sup>	$\mu_\delta$ mas yr <sup>-1</sup>	$v_{\text{rad}}$ km s <sup>-1</sup>	( $G$ , $G_{\text{BP}}$ , $G_{\text{RP}}$ ) mag	$T_{\text{eff}}$ K	Type	$N_{\text{Brv}}$
1	1042515801147259008	(129.799021, 62.501271)	0.39 ± 0.03	-33.08 ± 0.04	-41.03 ± 0.07	73.9 ± 1.1✓	(12.72, 13.26, 12.02)	4906 <sup>+263</sup> <sub>-114</sub>	K	25
2 <sup>M</sup>	1268023196461923712	(225.783582, 26.246320)	0.22 ± 0.02	-29.64 ± 0.04	-18.88 ± 0.04	-276.8 ± 1.6✓	(13.00, 13.49, 12.35)	4945 <sup>+383</sup> <sub>-80</sub>	K	7
3 <sup>M</sup>	1364548016594914560	(268.779224, 50.573050)	0.10 ± 0.02	-4.39 ± 0.04	7.82 ± 0.04	110.4 ± 0.4✓	(11.93, 12.56, 11.20)	4813 <sup>+221</sup> <sub>-262</sub>	K	10
4 <sup>B,M</sup>	2106519830479009920	(285.484415, 45.971657)	0.12 ± 0.02	3.30 ± 0.04	13.17 ± 0.04	-212.1 ± 1.0✓	(12.42, 13.04, 11.69)	4830 <sup>+107</sup> <sub>-162</sub>	K	8
5	2233912206910720000	(299.283801, 55.496959)	0.28 ± 0.02	27.85 ± 0.03	-5.48 ± 0.03	-343.9 ± 1.7✓	(12.97, 13.41, 12.36)	5158 <sup>+802</sup> <sub>-80</sub>	G	11
6 <sup>B,M</sup>	3705761936916676864	(192.764203, 4.941087)	0.27 ± 0.02	15.04 ± 0.05	-32.29 ± 0.03	88.7 ± 1.9✓	(13.19, 13.66, 12.57)	5036 <sup>+125</sup> <sub>-176</sub>	G	17
7 <sup>M</sup>	3784964943489710592	(169.356296, -5.815378)	0.26 ± 0.04	22.58 ± 0.08	-16.33 ± 0.05	126.2 ± 1.3✓	(12.25, 12.76, 11.58)	4997 <sup>+89</sup> <sub>-84</sub>	K	9
8	4136024785619932800	(258.736351, -16.502178)	0.51 ± 0.09	-1.25 ± 0.15	-8.23 ± 0.10	496.5 ± 4.8✓	(16.55, 17.04, 15.90)	4940 <sup>+117</sup> <sub>-158</sub>	K	2
9	4248140165233284352	(299.667995, 4.511052)	0.15 ± 0.02	-17.34 ± 0.03	-0.19 ± 0.03	-358.1 ± 2.3✓	(13.21, 13.75, 12.52)	4859 <sup>+72</sup> <sub>-72</sub>	K	7
10	4593398670455374592	(274.896548, 33.818936)	0.20 ± 0.02	-1.18 ± 0.04	-25.74 ± 0.04	-313.0 ± 1.2✓	(12.24, 12.67, 11.65)	5470 <sup>+775</sup> <sub>-442</sub>	K	8
11 <sup>M</sup>	4916199478888664320	(23.382529, -51.923180)	0.18 ± 0.02	-11.09 ± 0.03	-17.58 ± 0.04	86.9 ± 1.3✓	(12.61, 13.06, 11.99)	5052 <sup>+448</sup> <sub>-69</sub>	G	16
12 <sup>M</sup>	5212817273334550016	(107.199164, -76.219334)	0.26 ± 0.02	12.17 ± 0.04	35.92 ± 0.04	159.9 ± 0.3✓	(10.89, 11.66, 10.07)	4245 <sup>+160</sup> <sub>-83</sub>	K	8
13	5300505902646873088	(139.033697, -58.890109)	0.20 ± 0.01	13.98 ± 0.03	-16.88 ± 0.03	160.2 ± 4.0✓	(13.19, 13.87, 12.40)	4363 <sup>+90</sup> <sub>-136</sub>	K	3
14 <sup>M</sup>	5374177064347894272	(169.498826, -47.831289)	0.17 ± 0.02	7.24 ± 0.04	-17.28 ± 0.04	143.2 ± 0.5✓	(12.19, 12.85, 11.43)	4761 <sup>+320</sup> <sub>-106</sub>	K	17
15	5672759960942885376	(152.033666, -17.673459)	1.14 ± 0.05	-4.66 ± 0.09	6.23 ± 0.07	-332.5 ± 2.9✓	(15.58, 16.07, 14.92)	4999 <sup>+374</sup> <sub>-147</sub>	K	2
16	5808433545428565376	(253.529196, -68.655962)	0.15 ± 0.02	-12.04 ± 0.02	-21.48 ± 0.02	96.6 ± 1.0✓	(13.20, 13.83, 12.46)	4749 <sup>+157</sup> <sub>-164</sub>	K	6
17	6053231975369894400	(181.784844, -64.690105)	1.31 ± 0.07	-6.79 ± 0.12	-2.01 ± 0.09	-320.1 ± 2.6✓	(16.74, 17.45, 15.86)	4280 <sup>+106</sup> <sub>-85</sub>	K	2
18 <sup>M</sup>	6397497209236655872	(333.113416, -68.168596)	0.17 ± 0.02	-18.71 ± 0.02	-6.57 ± 0.02	-8.2 ± 3.6✓	(13.21, 13.68, 12.57)	5018 <sup>+454</sup> <sub>-89</sub>	G	8
19 <sup>B,M</sup>	6431596947468407552	(274.687922, -70.249323)	0.08 ± 0.02	4.55 ± 0.02	4.97 ± 0.02	259.1 ± 1.7✓	(13.09, 13.66, 12.38)	4834 <sup>+199</sup> <sub>-226</sub>	K	13
20	6433337199495213056	(279.867871, -67.154967)	0.14 ± 0.02	-4.15 ± 0.02	-21.85 ± 0.02	-89.9 ± 1.2✓	(13.00, 13.51, 12.33)	4893 <sup>+74</sup> <sub>-43</sub>	K	14
21	6625197335678814208	(334.068454, -25.560644)	0.21 ± 0.03	-7.02 ± 0.05	-27.30 ± 0.05	-399.8 ± 17.8✓	(13.02, 13.39, 12.46)	5295 <sup>+226</sup> <sub>-334</sub>	G	2
22	1995066395528322560	(359.273412, 56.883318)	0.80 ± 0.03	0.43 ± 0.04	0.69 ± 0.04	<b>-799.1 ± 1.1</b>	(13.32, 13.66, 12.81)	5745 <sup>+173</sup> <sub>-388</sub>	G	2
23	5916830097537967744	(256.319768, -57.362214)	0.44 ± 0.03	-1.05 ± 0.04	-0.57 ± 0.03	<b>-457.8 ± 1.5</b>	(13.33, 13.88, 12.57)	4861 <sup>+175</sup> <sub>-208</sub>	K	2

In the first column, the superscripts “B” and “M” indicate the sources which are listed in Bromley et al. (2018) and Marchetti et al. (2019), respectively. The variables are same as Table 1. The numbers shown in red are the *Gaia* measurements which are known to be erroneous for reasons given in Sect. 4, shown “as is”, without being corrected to their true physical values. Their unbound probabilities are shown in Table 4.

$$X_\phi = \frac{\cos(\tilde{\phi})}{\sigma_{\cos(\phi)}}, \quad (11)$$

where  $\cos(\tilde{\phi})$  is the median of  $\cos(\phi^t)$ .

To escape from the Galaxy, a binary must satisfy the following condition:

$$|v_{\text{grf}}| \geq |v_{\text{esc}}|. \quad (12)$$

The Galactic rest frame velocity  $v_{\text{grf}}$  of a binary can be obtained via the following relation:

$$v_{\text{grf}}^2 = av_s^2 + bv_s + c, \quad (13)$$

where  $a$ ,  $b$ , and  $c$  can be calculated using the coordinates, proper motions and parallax by means of a matrix (see Appendix 6). As shown in Equation (13),  $v_{\text{grf}}^2$  is a quadratic function of systemic radial velocity.

By substituting Equation (12) into Equation (13), the escaping condition can be written as follows:

$$\begin{cases} v_s \geq v_{\text{resc1}} = \frac{-b + \sqrt{b^2 - 4a(c - v_{\text{esc}}^2)}}{2a}, \\ \text{or} \\ v_s \leq v_{\text{resc2}} = \frac{-b - \sqrt{b^2 - 4a(c - v_{\text{esc}}^2)}}{2a}. \end{cases} \quad (14)$$

The minimum  $v_{\text{grf}}$  of the binary is larger than its  $v_{\text{esc}}$  when the relation  $b^2 - 4a(c - v_{\text{esc}}^2) < 0$  is satisfied. In this situation, the binary can always escape the Galaxy.

To calculate the unbound probability of the binary, the escaping condition is expressed with  $X_\phi$  (Eq. (10)):

$$\begin{cases} X_\phi \leq (\tilde{v}_{\text{rad}} - v_{\text{resc1}})/\sigma(v_{\text{rad}}^t), \\ \text{or} \\ X_\phi \geq (\tilde{v}_{\text{rad}} - v_{\text{resc2}})/\sigma(v_{\text{rad}}^t), \end{cases} \quad (15)$$

where  $\tilde{v}_{\text{rad}}$  and  $\sigma(v_{\text{rad}}^t)$  are the median and standard deviation of the radial velocities, respectively. According to Katz et al. (2019),

$$\sigma(v_{\text{rad}}^t) = \sqrt{\frac{2N}{\pi}(\epsilon_{v_{\text{rad}}}^2 - 0.11^2)}, \quad (16)$$

where  $\epsilon_{v_{\text{rad}}}$  is the radial velocity uncertainty (radial\_velocity\_error).

Since the orbital phases of the binary system are unknown, we assume that  $\phi^t$  follows a uniform distribution in the interval  $[0, 2\pi]$  and the binary is observed  $N$  times. We use the MC method to generate  $N$  random  $\phi^t$  to compute  $X_\phi$  with Equations (9) and (11) for each simulation. To obtain the probability density of  $f(X_\phi)$  for a fixed  $N$ ,  $10^6$  MC simulations are performed. Figure 2 shows an example of the probability density of  $X_\phi$  with MC simulations for different values of  $N$ .

According to our approach above, if the source that we investigated is a potential binary system, then its systemic radial escape velocity can be calculated with the median values of  $(\alpha, \delta, \varpi, \mu_\alpha, \mu_\delta)$ . The probability that the source

**Table 4** Unbound Probabilities of High Velocity Star Candidates with Median Radial Velocities

HV	$r_{GC}$ kpc	$v_{grf}$ km s <sup>-1</sup>	$v_{esc}$ km s <sup>-1</sup>	$P_{un}$	$N_{RP}$	$N_G$	GOOD	$RUWE$	$v_{30,esc}$ km s <sup>-1</sup>	$P_{30,un}$	$P_{\varpi+0.067,un}$
1	10.285 <sup>+0.205</sup> <sub>-0.170</sub>	518 <sup>+56</sup> <sub>-46</sub>	595 <sup>+2</sup> <sub>-2</sub>	0.100	0	0	✓	1.049	595 <sup>+30</sup> <sub>-30</sub>	0.124	0.001
2	7.753 <sup>+0.098</sup> <sub>-0.057</sub>	549 <sup>+78</sup> <sub>-62</sub>	616 <sup>+1</sup> <sub>-2</sub>	0.194	0	0	✓	1.061	616 <sup>+30</sup> <sub>-30</sub>	0.212	0.000
3	12.029 <sup>+1.934</sup> <sub>-1.177</sub>	534 <sup>+84</sup> <sub>-52</sub>	578 <sup>+10</sup> <sub>-14</sub>	0.304	0	0	✓	1.034	576 <sup>+32</sup> <sub>-33</sub>	0.320	0.000
4	10.190 <sup>+0.883</sup> <sub>-0.588</sub>	568 <sup>+87</sup> <sub>-65</sub>	595 <sup>+6</sup> <sub>-8</sub>	0.374	0	0	✓	1.024	594 <sup>+31</sup> <sub>-31</sub>	0.386	0.000
5	8.958 <sup>+0.097</sup> <sub>-0.081</sub>	540 <sup>+33</sup> <sub>-29</sub>	609 <sup>+1</sup> <sub>-1</sub>	0.028	0	0	✓	0.817	609 <sup>+30</sup> <sub>-30</sub>	0.067	0.000
6	8.357 <sup>+0.101</sup> <sub>-0.072</sub>	564 <sup>+59</sup> <sub>-48</sub>	611 <sup>+1</sup> <sub>-2</sub>	0.215	0	0	✓	0.996	611 <sup>+30</sup> <sub>-30</sub>	0.243	0.000
7	9.330 <sup>+0.342</sup> <sub>-0.272</sub>	530 <sup>+86</sup> <sub>-62</sub>	602 <sup>+3</sup> <sub>-2</sub>	0.203	0	0	✓	0.972	602 <sup>+30</sup> <sub>-30</sub>	0.217	0.006
8	6.390 <sup>+0.272</sup> <sub>-0.380</sub>	566 <sup>+6</sup> <sub>-6</sub>	641 <sup>+5</sup> <sub>-4</sub>	0.000	0	0	✓	1.013	642 <sup>+30</sup> <sub>-30</sub>	0.008	0.000
9	6.069 <sup>+0.303</sup> <sub>-0.086</sub>	572 <sup>+86</sup> <sub>-62</sub>	642 <sup>+2</sup> <sub>-5</sub>	0.212	0	0	✓	0.875	641 <sup>+30</sup> <sub>-30</sub>	0.226	0.000
10	7.492 <sup>+0.127</sup> <sub>-0.066</sub>	542 <sup>+73</sup> <sub>-58</sub>	623 <sup>+1</sup> <sub>-2</sub>	0.141	0	0	✓	0.907	623 <sup>+30</sup> <sub>-30</sub>	0.159	0.000
11	9.256 <sup>+0.374</sup> <sub>-0.260</sub>	533 <sup>+68</sup> <sub>-52</sub>	600 <sup>+3</sup> <sub>-4</sub>	0.173	0	0	✓	1.028	600 <sup>+30</sup> <sub>-30</sub>	0.194	0.000
12	8.099 <sup>+0.068</sup> <sub>-0.048</sub>	568 <sup>+58</sup> <sub>-50</sub>	617 <sup>+1</sup> <sub>-1</sub>	0.202	0	0	✓	0.878	617 <sup>+30</sup> <sub>-30</sub>	0.231	0.000
13	9.081 <sup>+0.142</sup> <sub>-0.139</sub>	582 <sup>+39</sup> <sub>-34</sub>	608 <sup>+2</sup> <sub>-2</sub>	0.259	0	0	✓	1.065	608 <sup>+30</sup> <sub>-30</sub>	0.307	0.000
14	8.682 <sup>+0.464</sup> <sub>-0.283</sub>	561 <sup>+88</sup> <sub>-65</sub>	611 <sup>+3</sup> <sub>-5</sub>	0.281	0	0	✓	1.023	610 <sup>+30</sup> <sub>-30</sub>	0.296	0.001
15	8.487 <sup>+0.011</sup> <sub>-0.010</sub>	564 <sup>+3</sup> <sub>-3</sub>	615 <sup>+0</sup> <sub>-0</sub>	0.000	0	0	✓	0.982	615 <sup>+30</sup> <sub>-30</sub>	0.046	0.000
16	5.384 <sup>+0.082</sup> <sub>-0.018</sub>	573 <sup>+87</sup> <sub>-70</sub>	651 <sup>+1</sup> <sub>-2</sub>	0.187	0	0	✓	0.992	650 <sup>+30</sup> <sub>-30</sub>	0.201	0.000
17	7.938 <sup>+0.015</sup> <sub>-0.010</sub>	546 <sup>+3</sup> <sub>-3</sub>	622 <sup>+0</sup> <sub>-0</sub>	0.000	0	0	✓	1.093	622 <sup>+30</sup> <sub>-30</sub>	0.006	0.000
18	6.825 <sup>+0.117</sup> <sub>-0.056</sub>	584 <sup>+52</sup> <sub>-42</sub>	626 <sup>+1</sup> <sub>-2</sub>	0.211	0	0	✓	1.120	626 <sup>+30</sup> <sub>-30</sub>	0.245	0.000
19	7.969 <sup>+2.180</sup> <sub>-1.243</sub>	607 <sup>+86</sup> <sub>-59</sub>	613 <sup>+15</sup> <sub>-21</sub>	0.475	0	0	✓	0.941	611 <sup>+34</sup> <sub>-36</sub>	0.482	0.000
20	5.253 <sup>+0.166</sup> <sub>-0.037</sub>	565 <sup>+88</sup> <sub>-69</sub>	649 <sup>+1</sup> <sub>-3</sub>	0.178	0	0	✓	0.931	648 <sup>+30</sup> <sub>-30</sub>	0.191	0.000
21	7.149 <sup>+0.122</sup> <sub>-0.028</sub>	563 <sup>+90</sup> <sub>-62</sub>	623 <sup>+3</sup> <sub>-1</sub>	0.247	0	0	✓	0.957	622 <sup>+30</sup> <sub>-30</sub>	0.262	0.002
22	8.877 <sup>+0.022</sup> <sub>-0.021</sub>	592 <sup>+1</sup> <sub>-1</sub>	611 <sup>+0</sup> <sub>-0</sub>	<b>0.000</b>	1	1		1.023	611 <sup>+30</sup> <sub>-30</sub>	<b>0.259</b>	<b>0.000</b>
23	6.369 <sup>+0.103</sup> <sub>-0.115</sub>	604 <sup>+1</sup> <sub>-1</sub>	642 <sup>+2</sup> <sub>-1</sub>	<b>0.000</b>	1	1		1.200	642 <sup>+30</sup> <sub>-30</sub>	<b>0.104</b>	<b>0.000</b>

The variables are same as Table 2.

could escape the Galaxy can then be written as follows:

$$P'_{un} = \begin{cases} \int_{-\infty}^{(\tilde{v}_{rad}-v_{resc1})/\sigma(v_{rad}^t)} f(X_\phi) dX_\phi, & (\tilde{v}_{rad} \geq v_{resc1}) \\ 0, & (v_{resc2} \geq \tilde{v}_{rad} \leq v_{resc1}) \\ \int_{(\tilde{v}_{rad}-v_{resc2})/\sigma(v_{rad}^t)}^{\infty} f(X_\phi) dX_\phi, & (\tilde{v}_{rad} \leq v_{resc2}) \end{cases} \quad (17)$$

and if  $b^2 - 4a(c - v_{esc}^2) < 0$ , then  $P'_{un} = 1$ .

Assuming that our 16 candidates are binary stars, we calculate their binary escape probabilities with the Galactic Potential Model I of Irrgang et al. (2013). The probabilities are invariably over 92% for all 16 objects, as shown in Figure 4 and Table 2. This means that if their radial velocity measurements can be assumed to be reliable, then all 16 would almost certainly be hypervelocity objects, whether or not they are in binary systems. However, since incorrect radial velocity measurements have a tendency to manifest themselves as outliers, and hence will be disproportionately represented among stars of high velocity, it would be folly to assume that such extreme cases do not exist in our sample. Consequently, we have no reason to assume that all radial velocity measurements are reliable, which is exactly the issue that we investigate in the next section.

#### 4 RADIAL VELOCITIES AND POSSIBLE CONTAMINATION

As previously noted, it was found by Boubert et al. (2019) that certain spectroscopic radial velocities obtained by

*Gaia* could be contaminated. They observed *Gaia* DR2 5932173855446728064 (*Gaia*-HVSC15 see Table 1) at eight epochs with a ground-based telescope, ultimately obtaining a median velocity of  $-56.5 \pm 5.3$  km s<sup>-1</sup> for the source, which is far slower than  $-614.3 \pm 2.5$  km s<sup>-1</sup> found by *Gaia* spectroscopy. They point out that, due to the slitless and time delay integration nature of *Gaia*, its results are likely to include the light from a close star (at 4.3 arcsec in their case), which is a potential source of contamination. Their studies also find that the radial velocity measurement will be spurious for any star that has a brighter ( $G$ - or  $G_{RP}$ -band) and closer (less than 6.4 arcsec) neighbor.

To test whether our sample suffers from the same issues, we observe one of our high velocity star candidates (HV22, see Table 3) using the Xinglong 2.16-m telescope. With a relatively bright magnitude of  $G = 13.32$  mag, it is impervious to issues arising from low signal to noise ratios (SNRs), and has a median radial velocity of  $-799.1 \pm 1.1$  km s<sup>-1</sup> and  $rv\_nb\_transits = 2$ , according to the *Gaia* catalogue.

HV22 was observed on 2019 January 27 using the BFOSC E9+G10 instrument of the Xinglong 2.16-m telescope at Xinglong Observatory (Zhao et al. 2018) with a 1.6 arcsec short slit. Its wavelength ranges from 3300 to 10000 Å, and we plot the part of the spectra with a relatively high SNR in Figure 5. Because the Balmer lines

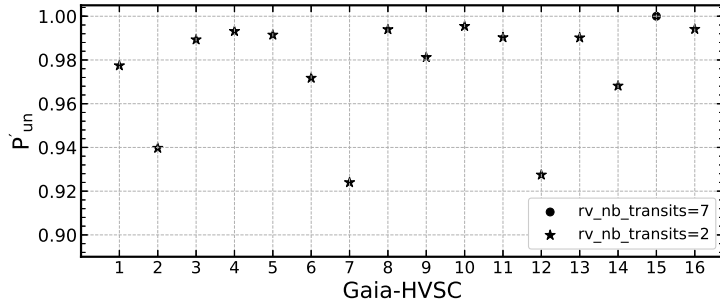


**Fig. 4** The Binary Escape Probabilities of the 16 sources, which have radial velocities in *Gaia* DR2, in the Galactic Potential Model I of Irrgang et al. (2013). The horizontal number indicates the HVS candidates’ number (see Table 2). *rv\_nb\_transits* is the number of transits (epochs) used to compute the medians and standard deviations of the radial velocities.

have good SNRs, we use Sersic profiles (see Eq. (18)) to fit them, and take the velocities corresponding to the centers of the absorption lines to be their radial velocities.

$$f(v) = 1 - I_0 e^{-(\frac{v-v_0}{\sigma})^n}, \quad (18)$$

where  $I_0$ ,  $v_0$ ,  $\sigma$  and  $n$  are free parameters for fitting Balmer lines. Physically speaking,  $v_0$  is the center velocity of an absorption line. For example, we fit the  $H_\beta$  line with the Sersic profile shown in Figure 6 and obtain a velocity of  $8.85 \text{ km s}^{-1}$ . Using the same method, we arrive at velocities of 0.08, 23.21, 50.85 and  $-54.66 \text{ km s}^{-1}$  for the  $H_\alpha$ ,  $H_\gamma$ ,  $H_\delta$ , and  $H_\epsilon$  lines, respectively. We then calculate a radial velocity of  $5 \pm 34 \text{ km s}^{-1}$  by using the mean and standard deviation of these five velocities from this spectrum. The radial velocity is much less than the absolute median radial velocity of *Gaia* DR2 ( $799.1 \pm 1.1 \text{ km s}^{-1}$ , see Table 3). This result confirms the findings of Boubert et al. (2019), that stars with close neighbors are subject to their spectral contamination, and subsequent spectroscopic radial velocities may not be as reliable as one might hope.

In Figure 7, we can see that there is a brighter star in the circle centered on HV22 with radius of 6.4 arcsec, and another star which is fainter by  $\sim 1 \text{ mag}$ . Therefore, its *Gaia* spectra have a high probability of being polluted by its neighbors, as was expected by Boubert et al. (2019).

The number of brighter stars around our HVS and high velocity star candidates within 6.4 arcsec are listed in Tables 2 and 4, respectively. In Table 4, we see that there is another high velocity candidate (HV23) having a brighter star within 6.4 arcsec. Its *Gaia* radial velocity ( $-457.8 \pm 1.5 \text{ km s}^{-1}$ ) is therefore unreliable and the Galactic rest frame velocity could hence be totally wrong. Moreover, the proper motions of these two high velocity candidates are very low, which implies that they are probably not high velocity stars. Finally, 21 high velocity candidates are left with possible “GOOD” radial velocities, as shown in Table 4. For our 16 HVS candidates, only five sources do not have brighter companions within 6.4 arcsec. Of these five remaining sources, we notice that there

are significantly bright stars just outside 6.4 arcsec of two of them, *Gaia*-HVSC11 (14.14 mag) and *Gaia*-HVSC12 (14.88 mag), whose *Gaia* spectra might also consequently be contaminated. We also eliminate these two objects from our candidate sample for good measure. Our final candidate sample consists of only *Gaia*-HVSC1, *Gaia*-HVSC2, and *Gaia*-HVSC3, which are consistent with having “GOOD” *Gaia* radial velocities (see Table 2).

## 5 DISCUSSION

In this paper, we employ a set of selection criteria to identify HVS candidates and high velocity candidates from *Gaia* DR2 sources which have good photometric and astrometric measurements. With an initial selection, we obtain 16 HVS candidates and 23 high velocity candidates.

Among our 16 HVS candidates, only one candidate (*Gaia* DR2 5932173855446728064, *Gaia*-HVSC15 in Table 2) is found amongst the 19 candidates listed by Marchetti et al. (2019). This is mainly because we use a slightly heavier potential model than theirs. Marchetti et al. (2019) use a four-component Galactic potential model to calculate the escape speed (Marchetti et al. 2019), which is lower than the  $v_{\text{esc}}$  obtained from the Galactic Potential Model I of Irrgang et al. (2013), as shown in Figure 1. Therefore, we find 10 of the 19 HVS candidates listed in Marchetti et al. (2019) to be merely high velocity candidates, instead of hypervelocity ones (see Sect. 2.2, Tables 3 and 4). On the other hand, Marchetti et al. (2019) and Bromley et al. (2018) select candidates with an additional condition  $rv\_nb\_transits > 5$ , which is not included in our selection criteria. This condition is based on the argument that if a source is just observed a few times ( $rv\_nb\_transits < 5$ ), it is possible that the median radial velocity of the source is caused by either the binary orbit or unreliable *Gaia* spectra. With this condition, our 15 HVS candidates are excluded. To account for any possible impact on our results due to uncertainties in the gravitational potential models, we repeat the process of calculating un-

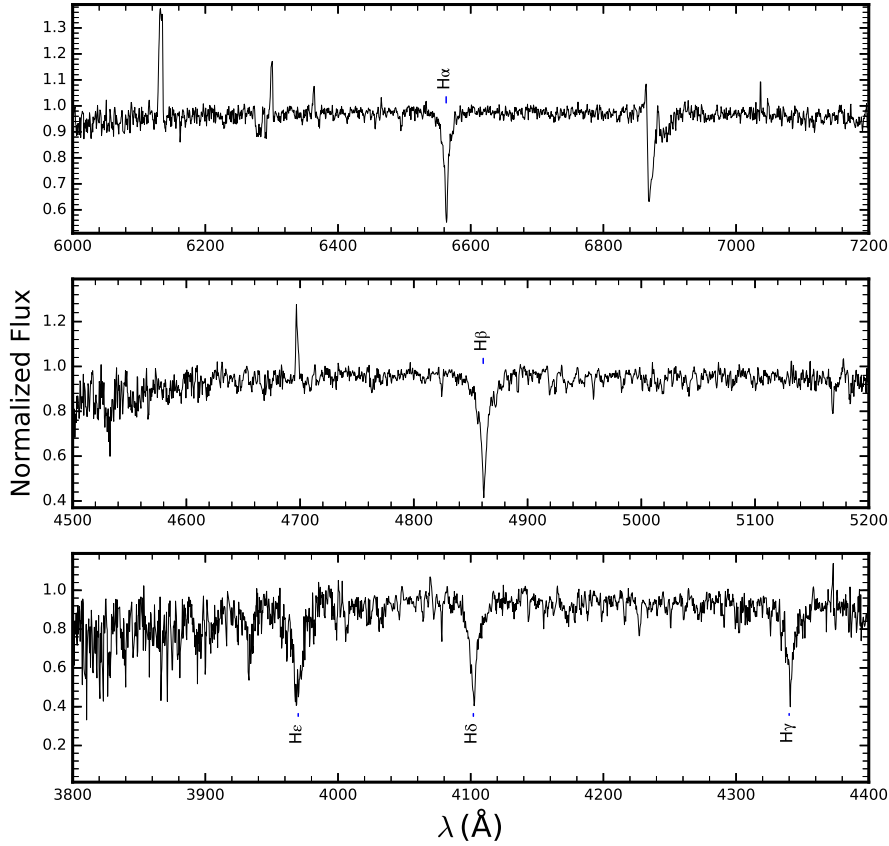


Fig. 5 Spectrum of HV22 (*Gaia* DR2 1995066395528322560).

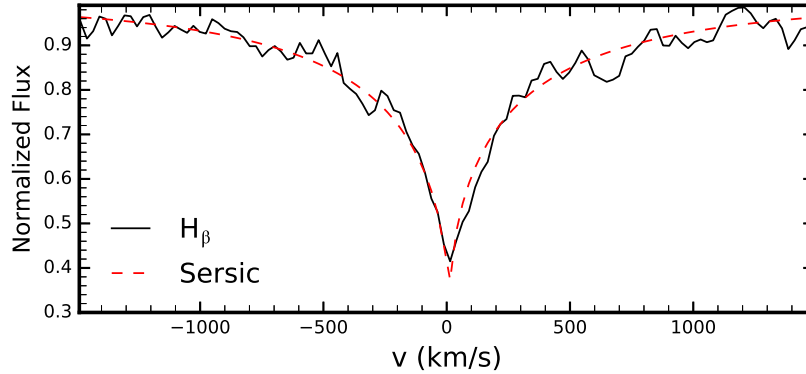
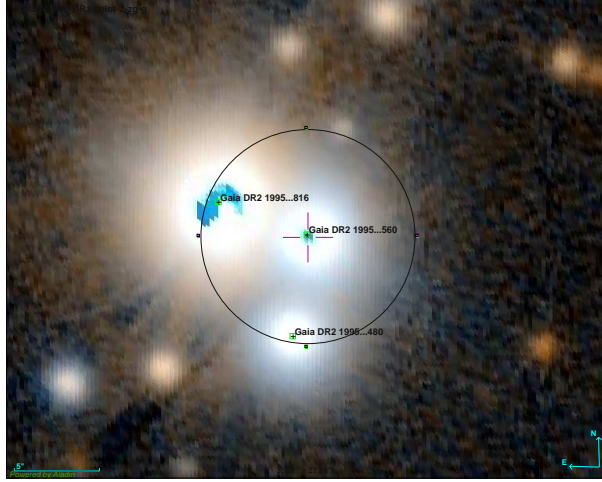


Fig. 6  $H_{\beta}$  line of HV22, fitted using a Sersic profile (Eq. (18)), where  $I_0$ ,  $v_0$ ,  $\sigma$ , and  $n$  are equal to 0.69, 8.85, 241.11 and 0.59, respectively. The radial velocity derived from this  $H_{\beta}$  line is  $8.85 \text{ km s}^{-1}$ .

bound probabilities for the objects in our sample, this time adding a Gaussian random error with a standard deviation of  $30 \text{ km s}^{-1}$  to the escape velocities. We chose the number  $30 \text{ km s}^{-1}$  because this is the escape velocity difference that one would expect from the gravitational potential models of Irrgang-II and Kenyon2018 depicted in Figure 1, at the typical distances ( $5 - 12 \text{ kpc}$ ) from the Galactic center for our sample objects. The results are also listed in Tables 2 and 4, where it can be seen that this has little af-

fect on our results. To investigate the unbound probabilities of the 15 candidates with few radial velocity measurement epochs ( $\text{rv\_nb\_transits} < 5$ ), which could potentially be binary components, we develop the BEPA approach. This approach estimates the unbound probabilities of the objects in question under the assumption that they indeed live in binary systems, which we find to be invariably greater than 92%. Therefore, it is prudent to include them in our HVS candidate sample.



**Fig. 7** PanSTARRS Image centered on GaiaVS22 (*Gaia* DR2 1995066395528322560) and downloaded from Aladin Desktop (<http://aladin.u-strasbg.fr>). The radius of the circle is 6.4 arcsec. The *Gaia* DR2 source IDs of the three bright stars in the *circle* are 1995066395528322816, 1995066395528322560, and 1995066395528324480; their *G*-band magnitudes are 11.85, 13.32, and 14.65 mag; their  $G_{RP}$ -band magnitudes are 11.02, 12.81 and 14.08 mag.

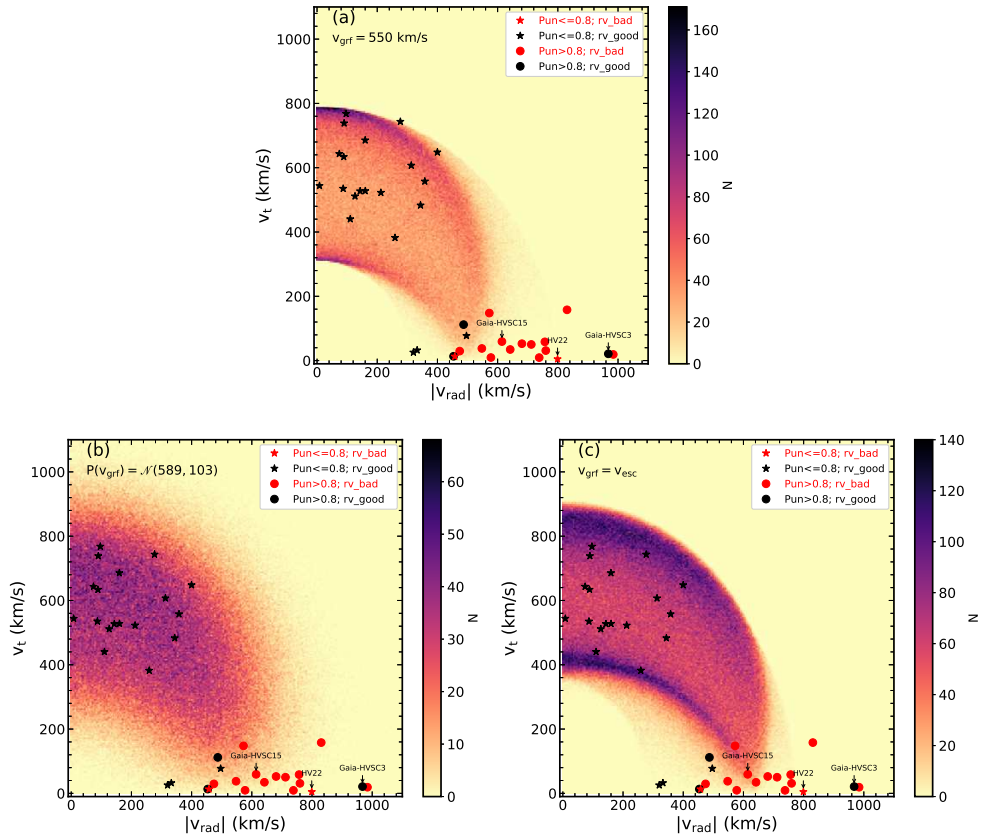


**Fig. 8** The radial velocity – transverse velocity diagram. The  $y$ - and  $x$ -axes are the tangential and radial velocity moduli, respectively. The *star-shaped markers* are the HVS candidates in Table 1; the *solid circles* are the high velocity candidates in Table 3; *black* and *red colors* are candidates with “GOOD” and “BAD” *Gaia* radial velocities, respectively (see Tables 2 and 4); *Gaia*-HVSC15 and HV22 are the sources observed by Boubert et al. (2019) and us using ground-based telescopes, respectively. The *color bar* indicates the number of simulated sources within each velocity bin (details in Sect. 6). The Galactic rest frame velocities of the simulated sources assumed in each panel are uniformly  $v_{\text{grf}} = 550 \text{ km s}^{-1}$  for (a), a Gaussian distribution with a mean of  $589 \text{ km s}^{-1}$  and a standard deviation of  $103 \text{ km s}^{-1}$  for (b), and equal to the local escape velocity of the sources for (c).

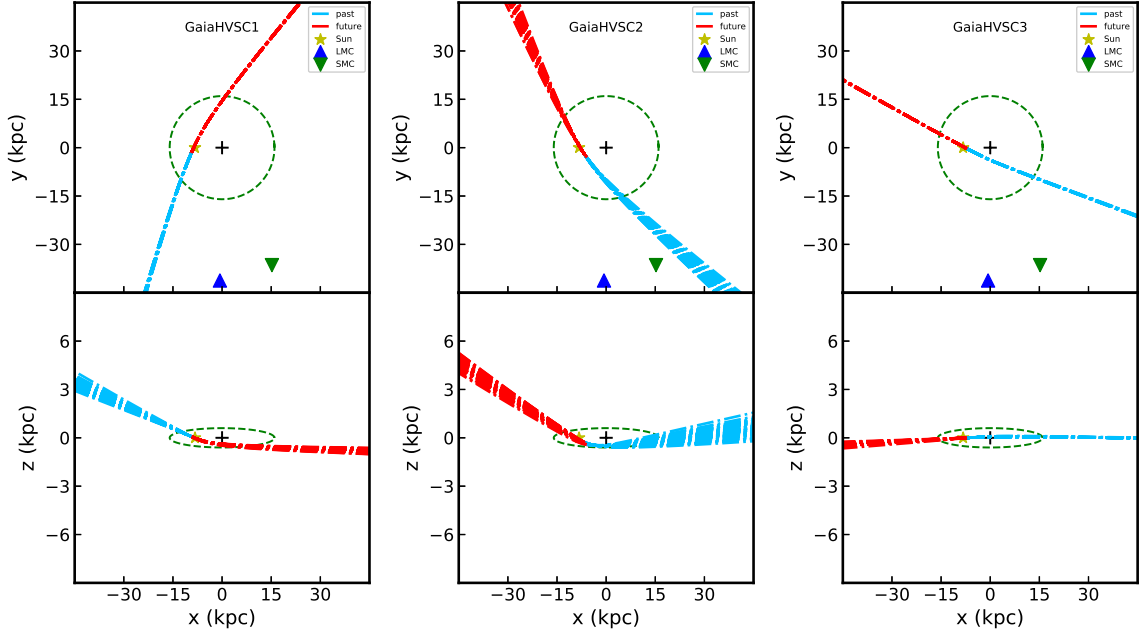


**Fig. 9** The integrated past (blue) and future (red) trajectories of the HVS candidates (*Gaia*-HVSC1, *Gaia*-HVSC2 and *Gaia*-HVSC3, see Table 2). The blue lines shown are integrated past trajectories, which do not take into account the position of birth of the star; all integrated past trajectories are integrated for 1 Gyr, regardless of the age of the star. The star marks the position of the Sun, while that of the GC, LMC, and SMC are denoted by a black plus sign, a blue triangle, and a green triangle, respectively. The edge of the Galactic disk at 16 kpc from the GC is marked with a green dashed circle. Both the  $x$ - $y$  plane and the  $x$ - $z$  plane are plotted for each object in question.

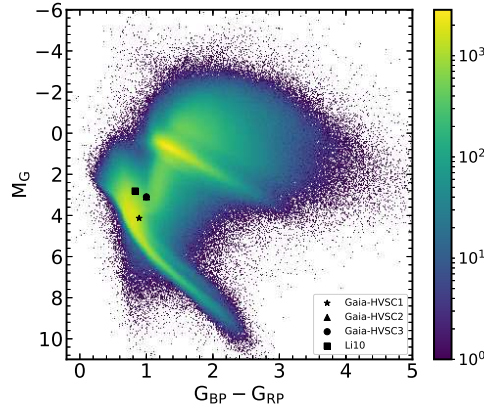


**Fig. 10** Hertzsprung-Russell (HR) density diagram for about 6.7 million objects which have radial velocities and  $\varpi > 5\sigma_\varpi$ . Black star, triangle and dot are HVS candidates *Gaia*-HVSC1, *Gaia*-HVSC2 and *Gaia*-HVSC3, respectively (see Table 1). Black square is HVS Li10 (Li et al. 2015; Boubert et al. 2018).

We also note that there is a systemic zero point offset of  $\sim -0.067$  mas in the *Gaia* parallaxes (Arenou et al. 2018). In order to estimate its influence on our candidates. We calculate the unbound probabilities with distances derived using  $1/(\varpi + 0.067 \text{ mas})$ . The unbound probabilities of the HVS candidates are still 1, but the high velocity star candidates are practically no longer able to escape the MW (see Tables 3 and 4).

However, the BEPA results hinge upon the measurements of the radial velocities, which can, in some cases,

be erroneous. For example, 5932173855446728064 (*Gaia*-HVSC15), a HVS candidate from Marchetti et al. (2019), was found to have an incorrect *Gaia* radial velocity determination (Boubert et al. 2019), due to a visible neighbor with similar or greater brightness than the star itself. We also observed HV22 ( $G = 13.32$  mag,  $rv\_nb\_transits = 2$ ) with the Xinglong 2.16-m telescope ourselves, and obtained a radial velocity of  $5 \pm 34 \text{ km s}^{-1}$ , which is much less than the median radial velocity of *Gaia* DR2 ( $-799.1 \pm 1.1 \text{ km s}^{-1}$ ). Its *Gaia* spectra are likely to be

contaminated by its two neighbors within 6.4 arcsec, which is consistent with the result of Boubert et al. (2019). After checking the neighbors of our candidates, only three HVS candidates and 21 high velocity candidates satisfy the condition of not suffering from such spectral contamination.

### 5.1 The Radial – Transverse Velocity Diagram of Candidates

To visualise our results, we plot our HVS candidates and high velocity star candidates on a radial velocity - transverse velocity plane (see Fig. 8). The objects that were found to have erroneous *Gaia* radial velocities are also plotted in red for comparison. In the plot, we can see clearly that most high velocity star candidates lie in areas of high transverse velocity and low radial velocity. Intuitively, this is largely due to velocity directions with higher transverse components taking up a greater solid angle than their high-radial-velocity counterparts. To test that this is indeed the case, we carry out the following experiment.

Noting that most of the candidates have parallaxes larger than 0.14 mas, corresponding to a solar-centric distance of  $\sim 7$  kpc, we artificially generate a mock sample of  $10^6$  stars within 7 kpc of the Sun, the number density of which follows that of Astraatmadja & Bailer-Jones 2016 and references therein. We also stochastically generate the velocities of these objects, assuming a fixed velocity magnitude of  $550 \text{ km s}^{-1}$  (which is the typical velocity of our high velocity star candidate sample), and a spherically random velocity distribution. The distribution of the velocities of these  $10^6$  objects relative to the Sun (accounting for solar motion relative to the Galactic Center) is plotted over our original sample in panel (a) of Figure 8. It can be seen that the bulk of these simulated objects indeed lie in the region where our high velocity star candidates are to be found. However, it should be noted that some of our sample data points lie beyond this distribution, whereas the lower half ( $160 \lesssim v_t \lesssim 360 \text{ km s}^{-1}$ ) of this distribution has no data points corresponding to it. Changing the way we generate our mock sample, either by assuming a Gaussian distribution for the velocity magnitudes (see panel (b) of Fig. 8), or by setting the velocities to the local escape velocity (see panel (c) of Fig. 8) does not change this trend. In other words, we do not expect the position of high velocity star candidates within the plane to be due to the previously mentioned solid angle effects alone.

What, then, causes our HVS candidates to lie outside the region covered by our mock sample? What denies the presence of high velocity star candidates in the lower half of the mock sample distribution? The answer is most probably selection effects – it is likely that either the way the *Gaia* mission was carried out, or the criteria we use to se-

lect our sample, has a tendency to neglect objects that lie in certain regions within this plot. If this interpretation is correct, then the existence of *Gaia* -HVSC3 implies the presence of a plethora of HVSs above the region covered by our mock samples in Figure 8. What the sources of these selection effects may be, however, is beyond the scope of this paper, and will be addressed in future work.

### 5.2 HVS Candidate Origins

To study the origins of HVSs, the simplest way is to trace the positions of our HVS sample back into the past via a set of dynamical calculations, thus obtaining a set of trajectories which shall henceforth be termed integrated past trajectories (IPTs).

Because we do not know when a particular HVS was originated, its past trajectories are integrated over a long timescale to include its birth positions. Had an HVS only just been born at a point in time  $t = t_0$ , then its IPT should also include its integrated positions prior to  $t_0$ .

We calculate the IPTs using the stellar kinematic code (Odenkirchen & Brosche 1992; Pauli et al. 2003, 2006), which calculates trajectories of point masses in the Galactic potential Model I of Irrgang et al. (2013) with a Bulirsch-Stoer integrator. The trajectories are integrated for 1 Gyr into the past, which we assume to be a generous upper limit to be the time that it would take for an unbound star to escape from the MW. We use a steplength of  $dt = 10^{-4}$  Gyr (Assuming a HVS with a velocity of  $1000 \text{ km s}^{-1}$ , it will move about 10 pc in every steplength).

If the unbound probability is less than 100%, then there exist trajectories which cannot escape the MW and would turn back to the Galaxy after a long travel time. Since we do not know the ages of the HVS candidates, it is difficult to determine where they originated from. This is different, however, for sources that are almost certainly unbound. From the trajectories, we can easily distinguish the origin of these HVS candidates.

In Figure 9, we plot the trajectories of “Good” HVS candidates. We account for the errors in the *Gaia* measurements by running a MC simulation generating the 3-D positions and velocities of these HVS candidates, which take into account the original *Gaia* data under the influence of their error bars. These velocities are then used to calculate the IPTs displayed in Figure 9, leading to the dispersion of IPTs evident in the figure. The integrated past and future trajectories are indicated by blue and red dash-dotted lines, respectively.

*Gaia*-HVSC1 moved from the bottom-right to top-left in the  $x$ - $y$  plane and has been traveling from the north to the south of MW. Judging by the fact that it never passed anywhere near the Galactic center, this candidate might ei-

ther have come from the disk or from the Halo of the MW. For *Gaia*-HVSC2 and *Gaia*-HVSC3, their past trajectories pass closer to the Galactic center, but not close enough for them to have originated there. From these IPTs, we have no reason to believe that any of these objects are from the Galactic center.

Examining the corresponding entries in the *Gaia* DR2 catalogue<sup>2</sup>, we find that *Gaia*-HVSC1, *Gaia*-HVSC2, and *Gaia*-HVSC1 have effective temperatures of about 5629 K (G-type), 5167 K (G-type), and 4166 K (K-type), respectively (see Table 1). Thus, the three HVS candidates are late type stars (see Fig. 10), similar to HVS Li10 (F-type, Li et al. 2015; Boubert et al. 2018). According to traditional wisdom, early (O, B and A) type HVSs are more likely to originate from the Galactic center (Lu et al. 2010; Brown 2015), whereas late-type stars can be born in either the Galactic center or the disk. If this is the case, then the spectral types of these objects are consistent with our earlier statement that they did not originate from the Galactic center, lending further credibility to our conclusions. It should be noted, however, that it has been recently found that a huge fraction of early type HVSs originate from the Galactic disk (Irrgang et al. 2018), therefore the correlation between the origin of an HVS and its spectral type appears to be a weak one. Further data may alter this status quo.

## 6 SUMMARY

We found three new late-type HVS candidates and 21 high velocity star candidates. Some of our high velocity star candidates are defined as HVS candidates in Marchetti et al. (2019). However, it should be noted that, for some of these new candidates, their *G*-band magnitudes can be close to 15 mag (see Tables 1 and 3), making them vulnerable to the issues raised in Katz et al. (2019), namely, that for sources with absolute radial velocities larger than 500 km s<sup>-1</sup>, their radial velocities may be unreliable in the presence of excessively low SNRs. To verify their status as HVSs and high velocity stars, future observations of these objects are necessary. As for the origins of these HVS candidates, we find it unlikely that any of them were born in the Galactic center.

**Acknowledgements** We thank David Katz, Douglas Boubert, Nami Mowlavi, Zhengwei Liu, Heran Xiong, Tommaso Marchetti, Hailiang Chen, Uli Bastian, Jan Rybizki and Haifeng Wang for valuable discussions. We thank Jianhua Wang and Qi Gao for helping us reduce spectra of HV22. This work has made use of data from the European Space Agency (ESA) mission *Gaia* (<https://www.cosmos.esa.int/gaia>), processed by the

*Gaia* Data Processing and Analysis Consortium (DPAC, <https://www.cosmos.esa.int/web/gaia/dpac/consortium>).

Funding for the DPAC has been provided by national institutions, in particular the institutions participating in the *Gaia* Multilateral Agreement. This work is supported by the Natural Natural Science Foundation of China (NSFC) (Grant Nos. 11521303, 11573061, 11733008 and 11661161016), by Yunnan province (2015FB190), by the Science and Technology Development Fund, Macau SAR (File Nos. 001/2016/AFJ and 0001/2019/A1). This project was developed in part at the 2018 GaiaLAMOST Sprint workshop, supported by the NSFC (Grant Nos. 11333003 and 11390372).

## Appendix A: 1

The Galactic rest frame velocity can be expressed as

$$\mathbf{v}_{\text{grf}} = \mathbf{R} \cdot \mathbf{v} + \mathbf{v}_{\odot}, \quad (\text{A.1})$$

where  $\mathbf{R} = \mathbf{T} \cdot \mathbf{A}$ , in which  $\mathbf{T}$  is the rotation matrix from equatorial coordinates to Galactic coordinates, and  $\mathbf{A}$  is the coordinate matrix of  $\mathbf{v}$  (details in Johnson & Soderblom 1987, the J2000 rotation matrix to Galactic coordinates is taken from the introduction to the Hipparcos catalog);  $\mathbf{v} = (v_s, \frac{k\mu_\alpha}{\varpi}, \frac{k\mu_\delta}{\varpi})^T$ , where  $k = 4.740470446$  km s<sup>-1</sup>, and  $\mathbf{v}_{\odot}$  is the Solar velocity in the Galactic rest frame. It follows that

$$v_{\text{grf}}^2 = av_s^2 + bv_s + c, \quad (\text{A.2})$$

where

$$\begin{aligned} a &= R_{11}^2 + R_{21}^2 + R_{31}^2, \\ b &= 2(R_{11}A + R_{21}B + R_{31}C), \\ c &= A^2 + B^2 + C^2, \end{aligned} \quad (\text{A.3})$$

and

$$\begin{aligned} A &= R_{12} \frac{k\mu_\alpha}{\varpi} + R_{13} \frac{k\mu_\delta}{\varpi} + v_{\odot 1}, \\ B &= R_{22} \frac{k\mu_\alpha}{\varpi} + R_{23} \frac{k\mu_\delta}{\varpi} + v_{\odot 2}, \\ C &= R_{32} \frac{k\mu_\alpha}{\varpi} + R_{33} \frac{k\mu_\delta}{\varpi} + v_{\odot 3}. \end{aligned} \quad (\text{A.4})$$

## References

- Abadi, M. G., Navarro, J. F., & Steinmetz, M. 2009, ApJ, 691, L63
- Allen, C., & Santillan, A. 1991, Rev. Mexicana Astron. Astrofis., 22, 255
- Arenou, F., Luri, X., Babusiaux, C., et al. 2018, A&A, 616, A17
- Astraatmadja, T. L., & Bailer-Jones, C. A. L. 2016, ApJ, 832, 137
- Blaauw, A. 1961, Bull. Astron. Inst. Netherlands, 15, 265
- Boubert, D., Erkal, D., Evans, N. W., & Izzard, R. G. 2017, MNRAS, 469, 2151
- Boubert, D., & Evans, N. W. 2016, ApJ, 825, L6

<sup>2</sup> <https://gea.esac.esa.int/archive/>

- Boubert, D., Guillochon, J., Hawkins, K., Ginsburg, I., & Evans, N. W. 2018, *MNRAS*, 479, 2789
- Boubert, D., Strader, J., Aguado, D., et al. 2019, *MNRAS*, 486, 2618
- Bromley, B. C., Kenyon, S. J., Brown, W. R., & Geller, M. J. 2018, *ApJ*, 868, 25
- Brown, W. R. 2006, *Bulletin of the American Astronomical Society*, 38, 1084
- Brown, W. R. 2015, *ARA&A*, 53, 15
- Brown, W. R., Geller, M. J., & Kenyon, S. J. 2009, *ApJ*, 690, 1639
- Brown, W. R., Geller, M. J., & Kenyon, S. J. 2012, *ApJ*, 751, 55
- Brown, W. R., Geller, M. J., & Kenyon, S. J. 2014, *ApJ*, 787, 89
- Brown, W. R., Geller, M. J., Kenyon, S. J., & Kurtz, M. J. 2005, *ApJ*, 622, L33
- Brown, W. R., Lattanzi, M. G., Kenyon, S. J., & Geller, M. J. 2018, *ApJ*, 866, 39
- Capuzzo-Dolcetta, R., & Fragione, G. 2015, *MNRAS*, 454, 2677
- Du, C., Li, H., Yan, Y., et al. 2019, *ApJS*, 244, 4
- Edelmann, H., Napiwotzki, R., Heber, U., Christlieb, N., & Reimers, D. 2005, *ApJ*, 634, L181
- Erkal, D., Boubert, D., Gualandris, A., Evans, N. W., & Antonini, F. 2019, *MNRAS*, 483, 2007
- Evans, D. W., Riello, M., De Angeli, F., et al. 2018, *A&A*, 616, A4
- Fritz, T. K., Battaglia, G., Pawlowski, M. S., et al. 2018, *A&A*, 619, A103
- Gaia Collaboration 2018, *Gaia Data Release 2 (DR2) gaia\_source Light*, VO Resource Provided by the GAVO Data Center
- Gaia Collaboration:, Brown, A. G. A., Vallenari, A., et al. 2018a, *A&A*, 616, A1
- Gaia Collaboration:, Helmi, A., van Leeuwen, F., et al. 2018b, *A&A*, 616, A12
- Gaia Collaboration:, Eyer, L., Rimoldini, L., et al. 2019, *A&A*, 623, A110
- Geier, S., Fürst, F., Ziegerer, E., et al. 2015, *Science*, 347, 1126
- Gvaramadze, V. V., Gualandris, A., & Portegies Zwart, S. 2009, *MNRAS*, 396, 570
- Hills, J. G. 1988, *Nature*, 331, 687
- Hirsch, H. A., Heber, U., O’Toole, S. J., & Bresolin, F. 2005, *A&A*, 444, L61
- Huang, Y., Liu, X.-W., Zhang, H.-W., et al. 2017, *ApJ*, 847, L9
- Irrgang, A., Kreuzer, S., & Heber, U. 2018, *A&A*, 620, A48
- Irrgang, A., Wilcox, B., Tucker, E., & Schiefelbein, L. 2013, *A&A*, 549, A137
- Johnson, D. R. H., & Soderblom, D. R. 1987, *AJ*, 93, 864
- Katz, D., Sartoretti, P., Cropper, M., et al. 2019, *A&A*, 622, A205
- Kenyon, S. J., Bromley, B. C., Brown, W. R., & Geller, M. J. 2014, *ApJ*, 793, 122
- Kenyon, S. J., Bromley, B. C., Brown, W. R., & Geller, M. J. 2018, *ApJ*, 864, 130
- Kenyon, S. J., Bromley, B. C., Geller, M. J., & Brown, W. R. 2008, *ApJ*, 680, 312
- Koposov, S. E., Boubert, D., Li, T. S., et al. 2019, *MNRAS*, DOI: 10.1093/mnras/stz3081
- Li, Y.-B., Luo, A.-L., Zhao, G., et al. 2015, *RAA (Research in Astronomy and Astrophysics)*, 15, 1364
- Li, Y., Luo, A., Zhao, G., et al. 2012, *ApJ*, 744, L24
- Lindegren, L., Hernández, J., Bombrun, A., et al. 2018, *A&A*, 616, A2
- Lu, Y., Zhang, F., & Yu, Q. 2010, *ApJ*, 709, 1356
- Marchetti, T., Contigiani, O., Rossi, E. M., et al. 2018, *MNRAS*, 476, 4697
- Marchetti, T., Rossi, E. M., & Brown, A. G. A. 2019, *MNRAS*, 490, 157
- Navarro, J. F., Frenk, C. S., & White, S. D. M. 1997, *ApJ*, 490, 493
- Odenkirchen, M., & Brosche, P. 1992, *Astronomische Nachrichten*, 313, 69
- Palladino, L. E., Schlesinger, K. J., Holley-Bockelmann, K., et al. 2014, *ApJ*, 780, 7
- Pauli, E.-M., Napiwotzki, R., Altmann, M., et al. 2003, *A&A*, 400, 877
- Pauli, E.-M., Napiwotzki, R., Heber, U., Altmann, M., & Odenkirchen, M. 2006, *A&A*, 447, 173
- Raddi, R., Hollands, M. A., Gänsicke, B. T., et al. 2018a, *MNRAS*, 479, L96
- Raddi, R., Hollands, M. A., Koester, D., et al. 2018b, *ApJ*, 858, 3
- Raddi, R., Hollands, M. A., Koester, D., et al. 2019, *MNRAS*, 489, 1489
- Schönrich, R. 2012, *MNRAS*, 427, 274
- Schönrich, R., Binney, J., & Dehnen, W. 2010, *MNRAS*, 403, 1829
- Shen, K. J., Boubert, D., Gänsicke, B. T., et al. 2018, *ApJ*, 865, 15
- Sohn, S. T., Watkins, L. L., Fardal, M. A., et al. 2018, *ApJ*, 862, 52
- Tauris, T. M. 2015, *MNRAS*, 448, L6
- Tauris, T. M., & Takens, R. J. 1998, *A&A*, 330, 1047
- Taylor, M. B. 2005, in *Astronomical Society of the Pacific Conference Series*, 347, *Astronomical Data Analysis Software and Systems XIV*, eds. P. Shopbell, M. Britton, & R. Ebert, 29
- Tillich, A., Przybilla, N., Scholz, R.-D., & Heber, U. 2009, *A&A*, 507, L37
- Vennes, S., Nemeth, P., Kawka, A., et al. 2017, *Science*, 357, 680
- Wang, B., & Han, Z. 2009, *A&A*, 508, L27
- Wang, B., Justham, S., & Han, Z. 2013, *A&A*, 559, A94
- Watkins, L. L., van der Marel, R. P., Sohn, S. T., & Evans, N. W. 2018, *ApJ*, 873, 118
- Wilkinson, M. I., & Evans, N. W. 1999, *MNRAS*, 310, 645
- Yu, Q., & Tremaine, S. 2003, *ApJ*, 599, 1129
- Zhang, F., Lu, Y., & Yu, Q. 2010, *ApJ*, 722, 1744
- Zhao, Y., Fan, Z., Ren, J.-J., et al. 2018, *RAA (Research in Astronomy and Astrophysics)*, 18, 110
- Zheng, Z., Carlin, J. L., Beers, T. C., et al. 2014, *ApJ*, 785, L23
- Zhong, J., Chen, L., Liu, C., et al. 2014, *ApJ*, 789, L2
- Ziegerer, E., Volkert, M., Heber, U., et al. 2015, *A&A*, 576, L14